

SYMPOL: SYMBOLIC TREE-BASED ON-POLICY REINFORCEMENT LEARNING

Sascha Marton*

University of Mannheim
Mannheim, Germany

sascha.marton@uni-mannheim.de

Tim Grams*

University of Mannheim
Mannheim, Germany

tim.nico.grams@uni-mannheim.de

Florian Vogt

University of Mannheim
Mannheim, Germany
fvogt@uni-mannheim.de

Stefan Lüdtke

University of Rostock
Rostock, Germany
luedtke@uni-rostock.de

Christian Bartelt

University of Mannheim
Mannheim, Germany
bartelt@uni-mannheim.de

Heiner Stuckenschmidt

University of Mannheim
Mannheim, Germany
stuckenschmidt@uni-mannheim.de

ABSTRACT

Reinforcement learning (RL) has seen significant success across various domains, but its adoption is often limited by the black-box nature of neural network policies, making them difficult to interpret. In contrast, symbolic policies allow representing decision-making strategies in a compact and interpretable way. However, learning symbolic policies directly within on-policy methods remains challenging. In this paper, we introduce SYMPOL, a novel method for SYMbolic tree-based on-POLicy RL. SYMPOL employs a tree-based model integrated with a policy gradient method, enabling the agent to learn and adapt its actions while maintaining a high level of interpretability. We evaluate SYMPOL on a set of benchmark RL tasks, demonstrating its superiority over alternative tree-based RL approaches in terms of performance and interpretability. To the best of our knowledge, this is the first method, that allows a gradient-based end-to-end learning of interpretable, axis-aligned decision trees on-policy. Therefore, SYMPOL can become the foundation for a new class of interpretable RL based on decision trees. Our implementation is available under: <https://github.com/s-marton/SYMPOL>.

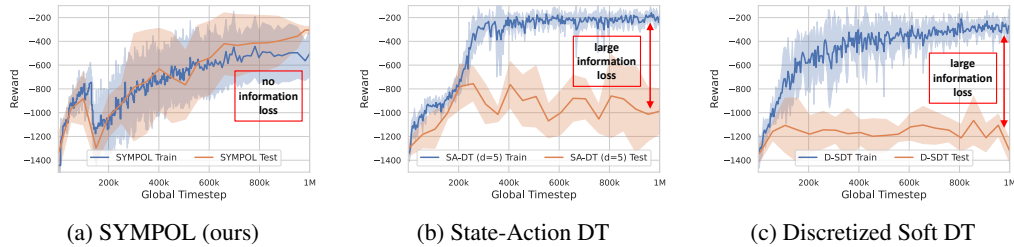


Figure 1: Information Loss in Tree-Based Reinforcement Learning on Pendulum. Existing methods for symbolic, tree-based RL (see Figure 1b and 1c) suffer from severe information loss when converting the differentiable policy (high train reward) into the symbolic policy (low test reward). Using SYMPOL (Figure 1a), we can directly optimize the symbolic policy with PPO and therefore have no information loss during the application (high train and test reward).

*Equal Contribution

1 INTRODUCTION

Reinforcement learning lacks transparency. Reinforcement learning (RL) has achieved remarkable success in solving complex sequential decision-making problems, ranging from robotics and autonomous systems to game playing and recommendation systems. However, the policies learned by traditional RL algorithms, represented by neural networks, often lack interpretability and transparency, making them difficult to understand, trust, and deploy in safety-critical or high-stakes scenarios (Landajuela et al., 2021).

Symbolic policies increase trust. Symbolic policies, on the other hand, offer a promising alternative by representing decision-making strategies in terms of RL policies as compact and interpretable structures (Guo et al., 2023). These symbolic representations do not only facilitate human understanding and analysis but also ensure predictable and explainable behavior, which is crucial for building trust and enabling effective human-AI collaboration. Moreover, the deployment of symbolic policies in safety-critical systems, such as autonomous vehicles or industrial robots, could significantly improve their reliability and trustworthiness. By providing human operators with a clear understanding of the decision-making process, symbolic policies can facilitate effective monitoring, intervention, and debugging, ultimately enhancing the safety and robustness of these systems. In this context, decision trees (DTs) are particularly effective as symbolic policies for RL, as their hierarchical structure provides natural interpretability.

Existing challenges. Despite these promising prospects, the field of symbolic RL faces several challenges. One main reason is given by the fact that many symbolic models, like DTs, are non-differentiable and cannot be integrated in existing RL frameworks. Therefore, traditional methods for learning symbolic policies often rely on custom and complex training procedures (Costa et al., 2024; Vos & Verwer, 2023; Kanamori et al., 2022), limiting their applicability and scalability. Alternative methods involve pre-trained neural network policies combined with some post-processing to obtain an interpretable model (Silva et al., 2020; Liu et al., 2019; 2023; Bastani et al., 2018). However, post-processing introduces a mismatch between the optimized policy and the model obtained for interpretation, which can lead to loss of crucial information, as we show in Figure 1.

Contribution. In this paper, we introduce SYMPOL, SYMbolic tree-based on-POLicy RL, a novel method for efficiently learning interpretable, axis-aligned DT policies end-to-end (Section 4.1). Therefore, we use GradTree (Marton et al., 2024a) to directly optimize DTs with policy gradients. Unlike other approaches, SYMPOL does not depend on pre-trained neural network policies, complex search procedures, or post-processing steps, but can be seamlessly integrated into existing actor-critic RL algorithms, such as proximal policy optimization (Section 3). Since using DTs as policies can increase the risk of unstable training, we additionally propose a dynamic rollout buffer to enhance exploration stability and a dynamic batch size through gradient accumulation to improve gradient stability (Section 4.2). To the best of our knowledge, SYMPOL is the first method to facilitate a direct, end-to-end optimization of axis-aligned DT policies within arbitrary on-policy RL frameworks. While existing methods for learning DT policies, such as those described by Silva et al. (2020), suffer from information loss due to post-hoc distillation or discretization (see Figure 1), SYMPOL guarantees that the learned policy remains consistent from training to inference.

Results. Through extensive experiments on benchmark RL environments, we demonstrate that SYMPOL outperforms existing tree-based RL approaches in terms of interpretability and performance (Section 5.2), providing human-understandable explanations for its decision-making process. Furthermore, we provide a case study (Section 6) to show how interpretable policies help in detecting misbehavior and misgeneralization which might remain unnoticed with commonly used black-box policies.

2 RELATED WORK

Recently, the integration of symbolic methods into RL has gained significant attention. While symbolic RL does cover different approaches including program synthesis (Trivedi et al., 2021; Penkov & Ramamoorthy, 2019; Verma et al., 2018), concept bottleneck models (Ye et al., 2024), piecewise linear networks (Wabbartha & Pineau, 2024), logic (Delfosse et al., 2024), mathematical expressions (Landajuela et al., 2021; Guo et al., 2024; Luo et al., 2024; Xu et al., 2022), we focus on tree-based methods in this paper. Several approaches have been proposed to leverage the strengths of inter-

pretable, tree-based representations within RL frameworks. However, each approach comes with its own critical limitations. We summarize existing methods into three streams of work:

(1) Post-processing. One line learns full-complexity policies first and then performs some kind of post-processing for interpretability. One prominent example is the VIPER algorithm (Bastani et al., 2018). In this case, a policy is learned using neural networks before DTs are distilled from the policy. However, distillation methods often suffer from significant performance mismatches between the training and evaluation policies (see Figure 1b). To mitigate this mismatch, existing methods often learn large DTs (VIPER learns DTs with 1,000 nodes) and therefore aim for systematic verification rather than interpretability. In contrast, SYMPOL is able to learn small, interpretable DTs (average of only 50 nodes) without information loss. Following VIPER, various authors proposed similar distillation methods (Li et al., 2021; Liu et al., 2019; 2023; Jhunjhunwala et al., 2020).

(2) Soft Decision Trees (SDTs). Methods optimizing SDTs are difficult to interpret due to missing hard and axis-aligned properties (Silva et al., 2020; Silva & Gombolay, 2021; Coppens et al., 2019; Tambwekar et al., 2023). As SDTs model probability distributions in their internal nodes and, therefore, allow gradient optimization, they can be integrated into existing RL frameworks. Nevertheless, the trees are usually not easily interpretable and techniques such as discretizing the learned trees into more interpretable representations are applied (Silva et al., 2020), occasionally resulting in high performance mismatches (Figure 1c). In contrast, SYMPOL directly optimizes hard, axis-aligned DTs and therefore does not exhibit a performance loss (Figure 1a).

(3) Custom optimization. The third line involves custom, tree-specific optimization techniques and/or objectives (Ernst et al., 2005; Roth et al., 2019; Gupta et al., 2015; Kanamori et al., 2022) and, hence, is more time-consuming and less flexible. As a result, their policy models cannot be easily integrated into existing learning RL frameworks. Examples are evolutionary methods (Costa et al., 2024; Custode & Iacca, 2023) and linear integer programming (Vos & Verwer, 2023).

Furthermore, trees have also been used in other agentic components than the policy, such as reward functions (Milani et al., 2022; Kalra & Brown, 2023; 2022). Similarly, ensemble methods (Fuhrer et al., 2024; Min & Elliott, 2022) have been proposed. However, policies consisting of hundreds of trees and nodes lack interpretability and therefore are out of scope for this paper.

3 PRELIMINARIES

Markov Decision Process. We study a discounted Markov decision process $(\mathcal{S}, \mathcal{A}, \mathcal{P}, r, \gamma)$ where \mathcal{S} is a finite state space, \mathcal{A} is the finite action space, $\mathcal{P} : \mathcal{S} \times \mathcal{A} \times \mathcal{S} \rightarrow [0, 1]$ defines the transition dynamics of the environment, $r : \mathcal{S} \times \mathcal{A} \rightarrow \mathbb{R}$ is the reward function and γ the discount factor. At each timestep t , an agent samples an action from policy $\pi : \mathcal{S} \rightarrow \mathcal{A}$ based on the current observation $s_t \in \mathcal{S}$ and executes it in the environment. The environment transitions and the agent receives a reward r_t . In this context, the value function $\mathcal{V}^\pi(s) = \mathbb{E}_{a_t \sim \pi, s_{t+1} \sim \mathcal{P}} [\sum_{t=0}^{\infty} \gamma^t r(s_t, a_t) | s_t = s]$ approximates the expected return when starting in state s and then acting according to policy π . Similarly, the action-value function $\mathcal{Q}^\pi(s, a) = \mathbb{E}_{a_t \sim \pi, s_{t+1} \sim \mathcal{P}} [\sum_{t=0}^{\infty} \gamma^t r(s_t, a_t) | s_t = s, a_t = a]$ estimates the expected return when selecting action a in state s and then following policy π . Finally, the advantage function $\mathcal{A}^\pi(s, a) = \mathcal{Q}^\pi(s, a) - \mathcal{V}^\pi(s)$ defines the difference between the expected return when choosing action a in state s and the expected return when following the policy π from state s . Overall, we aim for finding an optimal policy π^* that maximizes the expected discounted return $J(\pi) = \mathbb{E} [\sum_{t=0}^{\infty} \gamma^t r(s_t, a_t)]$.

Proximal Policy Optimization (PPO). PPO (Schulman et al., 2017) is an actor-critic policy gradient method designed to enhance the stability of training dynamics. The algorithm introduces a clipped surrogate objective to restrict the policy update step size. The main idea is to constrain policy changes to a small trust region, preventing large updates that could destabilize training. Formally, PPO optimizes:

$$\mathcal{L}^{\text{CLIP}}(\theta) = \mathbb{E}_{a_t \sim \pi_{\theta_{\text{old}}}, s_{t+1} \sim \mathcal{P}} \left[\min \left(\frac{\pi_{\theta}(a_t | s_t)}{\pi_{\theta_{\text{old}}}(a_t | s_t)} \hat{A}_t, \text{clip} \left(\frac{\pi_{\theta}(a_t | s_t)}{\pi_{\theta_{\text{old}}}(a_t | s_t)}, 1 - \epsilon, 1 + \epsilon \right) \hat{A}_t \right) \right] \quad (1)$$

where $\frac{\pi_{\theta}(a_t | s_t)}{\pi_{\theta_{\text{old}}}(a_t | s_t)}$ is the probability ratio between the new policy π_{θ} and old policy $\pi_{\theta_{\text{old}}}$. \hat{A}_t is an estimate of the advantage function at time step t and ϵ is a hyperparameter for the clipping range.

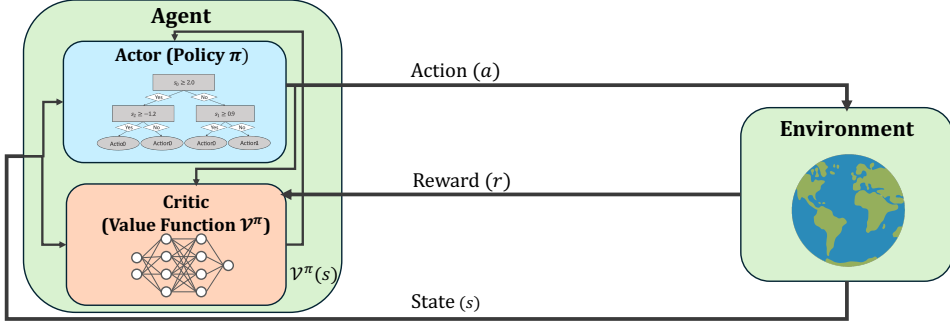


Figure 2: **SYMPOL**. This is an overview of SYMPOL, with its two main components: (1) an interpretable DT policy and (2) a neural network as critic.

4 SYMPOL: SYMBOLIC ON-POLICY RL

In the following, we formalize the online training of hard, axis-aligned DTs¹ with the PPO objective. In contrast to existing work on RL with DTs, this allows an optimization of the DT on-policy without information loss. Our method can be combined with arbitrary gradient-based RL frameworks. In this paper we study PPO as the, we believe, most prominent method to date and leave other methods for further research. To efficiently learn DT policies with SYMPOL, we employed several crucial (see ablation study in Table 5) modifications, which we will elaborate below.

4.1 LEARNING DTs WITH POLICY GRADIENTS

SYMPOL utilizes GradTree (Marton et al., 2024a) as a core component to learn a DT policy. In the following section, we incorporate GradTree into the PPO framework.

Arithmetic DT policy formulation. Traditionally, DTs involve nested concatenations of rules. In GradTree, DTs are formulated as arithmetic functions based on addition and multiplication to facilitate gradient-based learning. Therefore, our resulting DT policy is fully-grown (i.e., complete, full) and can be pruned post-hoc. Our basic pruning involves removing redundant paths, which significantly reduces the complexity. We define a path as redundant if the decision is already determined either by previous splits or based on the range of the selected feature. More details are given in Section A.2. Overall, we formulate a DT policy π of depth d with respect to its parameters as:

$$\pi(s|\mathbf{a}, \boldsymbol{\tau}, \boldsymbol{\iota}) = \sum_{l=0}^{2^d-1} a_l \mathbb{L}(s|l, \boldsymbol{\tau}, \boldsymbol{\iota}) \quad (2)$$

where \mathbb{L} is a function that indicates whether a state $s \in \mathbb{R}^{|\mathcal{S}|}$ belongs to a leaf l , $\mathbf{a} \in \mathcal{A}^{2^d}$ denotes the selected action for each leaf node, $\boldsymbol{\tau} \in \mathbb{R}^{2^d-1}$ represents split thresholds and $\boldsymbol{\iota} \in \mathbb{N}^{2^d-1}$ the feature index for each internal node.

Dense architecture. To support a gradient-based optimization and ensure an efficient computation via matrix operations, we make use of a dense DT representation. Traditionally, the feature index vector $\boldsymbol{\iota}$ is one-dimensional. However, as in GradTree, we expand it into a matrix form. Specifically, this representation one-hot encodes the feature index, converting $\boldsymbol{\iota} \in \mathbb{R}^{2^d-1}$ into a matrix $\mathbf{I} \in \mathbb{R}^{(2^d-1) \times |\mathcal{S}|}$. Similarly, for split thresholds, instead of a single value for all features, individual values for each feature are stored, leading to $\mathbf{T} \in \mathbb{R}^{(2^d-1) \times |\mathcal{S}|}$. By enumerating the internal nodes in breadth-first order, we can redefine the indicator function \mathbb{L} for a leaf l , resulting in

$$\pi(s|\mathbf{a}, \mathbf{T}, \mathbf{I}) = \sum_{l=0}^{2^d-1} a_l \mathbb{L}(s|l, \mathbf{T}, \mathbf{I}) \quad (3)$$

¹In the following, we will refer to hard, axis-aligned DTs simply as *DTs*, and specifically note exceptions.

$$\text{where } \mathbb{L}(\mathbf{s}|l, \mathbf{T}, \mathbf{I}) = \prod_{j=1}^d (1 - \mathbf{p}(l, j)) \mathbb{S}(\mathbf{s}|\mathbf{I}_{i(l,j)}, \mathbf{T}_{i(l,j)}) + \mathbf{p}(l, j) (1 - \mathbb{S}(\mathbf{s}|\mathbf{I}_{i(l,j)}, \mathbf{T}_{i(l,j)})) \quad (4)$$

Here, i is the index of the internal node preceding a leaf node l at a certain depth j and \mathbf{p} indicates whether the left ($\mathbf{p} = 0$) or the right branch ($\mathbf{p} = 1$) was taken.

Axis-aligned splitting. Typically, DTs use the Heaviside function for splitting, which is non-differentiable. We use the split function introduced in GradTree to account for reasonable gradients:

$$\mathbb{S}(\mathbf{s}|\boldsymbol{\iota}, \boldsymbol{\tau}) = \lfloor S(\boldsymbol{\iota} \cdot \mathbf{s} - \boldsymbol{\iota} \cdot \boldsymbol{\tau}) \rfloor \quad (5)$$

where $S(z) = \frac{1}{1+e^{-z}}$ represents the logistic function, $\lfloor z \rfloor$ stands for rounding a real number z to the nearest integer and $\boldsymbol{a} \cdot \boldsymbol{b}$ denotes the dot product. We further need to ensure that $\boldsymbol{\iota}$ is a one-hot encoded vector to account for axis-aligned splits. This is achieved by applying a hardmax transformation before calculating \mathbb{S} . Both rounding and hardmax operations are non-differentiable. To overcome this, we employ a straight-through operator (Bengio et al., 2013) during backpropagation. This allows the model to use non-differentiable operations in the forward pass while ensuring gradient propagation in the backward pass.

Weight decay. In contrast to GradTree, which employs an Adam (Kingma & Ba, 2014) optimizer with stochastic weight averaging (Izmailov et al., 2018), we opted for an Adam optimizer with weight decay (Loshchilov & Hutter, 2017). In the context of SYMPOL, weight decay does not serve as a direct regularizer for model complexity as it does in standard neural networks, since the interpretation of model parameters differs. We distinguish between three types of parameters: the predicted distributions in the leaves (\mathbf{a}), the split index encoding (\mathbf{I}), and the split values (\mathbf{T}). We do not apply weight decay to the split values because their significance is independent of magnitude. However, for the split indices and leaves, weight decay facilitates exploration during training by penalizing large parameter values, thereby maintaining a balanced distribution. This aids in dynamically adjusting which feature is considered at a split and in altering the class predictions at the leaves. Additionally, we decrease the learning rate if no improvement in validation reward is observed for five consecutive iterations, allowing for finer model adjustments in later training stages.

Actor-critic network architecture. Commonly, the actor and critic use a similar network architecture or even share the same weights (Schulman et al., 2017). While SYMPOL aims for a simple and interpretable policy, we do not have the same requirements for the critic. Therefore, we decided to only employ a tree-based actor and use a full-complexity neural network as a value function. Therefore, we can still capture complexity through the value function, without loosing interpretability as we maintain a simple and interpretable policy. We visualized the concept of SYMPOL in Figure 2.

Continuous action spaces. Furthermore, we extend the DT policy of SYMPOL to environments with continuous action spaces. Therefore, instead of predicting a categorical distribution over the classes, we predict the mean of a normal distribution at each leaf and utilize an additional variable $\sigma_{\log} \in \mathbb{R}^{|\mathcal{A}|}$ to learn the log of the standard deviation.

4.2 ADDRESSING TRAINING STABILITY

One main challenge when using DTs as a policy is the stability. While a stable training is also desired and often hard to achieve for a neural network policy, this is even more pronounced for SYMPOL. This is mainly caused by the inherent tree-based architecture. Changing a split at the top of the tree can have a severe impact on the whole model, as it can completely change the paths taken for certain observations. This is especially relevant in the context of RL, where the data distribution can vary highly between iterations. To mitigate the impact of highly non-stationary training samples, especially at early stages of training, we made two crucial modifications for improved stability of SYMPOL.

Exploration stability. Motivated by the idea that rollouts of more accurate policies contain increasingly diverse, higher quality samples, we implemented a dynamic number of environment steps between training iterations. Let us consider a pendulum as an example. While at early stages of training a relatively small sample size facilitates faster learning as the pendulum constantly flips, more optimal policies lead to longer rollouts and therefore more expressive and diverse experiences in the rollout buffer. Similarly, the increasing step counts stabilize the optimization of policy and critic, as the number of experiences for gradient computation grow with agent expertise and capture the diversity within trajectories better. Therefore, our novel collection approach starts with n_{init} environment steps and expands until n_{final} actions are taken before each training iteration. For computational efficiency reasons, instead of increasing the size of the rollout buffer at every time step, we introduce a stepwise exponential function (Figure 3). The exponential increase supports exploration in the initial iterations, while maintaining stability at later iterations. Hence, we define the number of steps in the environment n_t at time step t as

$$n_t = n_{\text{init}} \times 2^{\lfloor \frac{(t+1) \times i}{1+t_{\text{total}}} \rfloor - 1} \text{ with } i = 1 + \log_2 \left(\frac{n_{\text{final}}}{n_{\text{init}}} \right) \quad (6)$$

For our experiments, we define n_{init} as a hyperparameter (similar to the static step size for other methods) and set $n_{\text{final}} = 128 \times n_{\text{init}}$ and therefore $i = 8$ which we observed is a good default value.

Gradient stability. We also utilize large batch sizes for SYMPOL resulting in less noisy gradients, leading to a smoother convergence and better stability. In this context, we implement gradient accumulation to virtually increase the batch size further while maintaining memory-efficiency. As reduced noise in the gradients also leads to less exploration in the parameter space, we implement a dynamic batch size, increasing in the same rate as the environment steps between training iterations (Equation 6). Therefore, we can benefit from exploration and fast convergence early on and increase gradient stability during the training.

5 EVALUATION

We designed our experiments to evaluate whether SYMPOL can learn accurate DT policies without information loss and observe whether the trees learned by SYMPOL are small and interpretable. Furthermore, we conducted an ablation study to show how the proposed design choices (Section 4) affect the performance.

5.1 EXPERIMENTAL SETTINGS

Setup. We implemented SYMPOL in a highly efficient single-file JAX implementation that allows a flawless integration with highly optimized training frameworks (Lange, 2022; Weng et al., 2022; Bonnet et al., 2024). We evaluated our method on several environments commonly used for benchmarking RL methods. Specifically, we used control environments including CartPole (CP), Acrobat (AB), LunarLander (LL), MountainCarContinuous (MC-C) and Pendulum (PD-C), as well as the MiniGrid (Chevalier-Boisvert et al., 2023) environments Empty-Random (E-R), DoorKey (DK), LavaGap (LG) and DistShift (DS).

Methods. The goal of this evaluation is to compare SYMPOL to alternative methods that allow an interpretation of RL policies as a symbolic, axis-aligned DTs. Therefore, we build on previous work (Silva et al., 2020) and use two methods grounded in the interpretable RL literature, as follows:

- **State-Action DTs (SA-DT):** Behavioral cloning SA-DTs are the most common method to generate interpretable policies post-hoc. Hereby, we first train an MLP policy, which is then distilled into a DT as a post-processing step after the training.

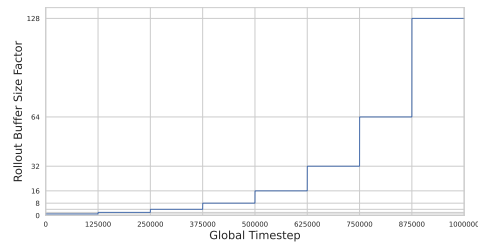


Figure 3: Rollout Size Factor by Global Timestep. This figure shows how the factor by which the rollout buffer size (= the number of environment steps per training iteration) is multiplied increases at a stepwise exponential rate over time.

- **Discretized Soft DTs (D-SDT):** SDTs allow gradient computation by assigning probabilities to each node. While SDTs exhibit a hierarchical structure, they are usually considered as less interpretable, since multiple features are considered in a single split and the whole tree is traversed simultaneously (Marton et al., 2024a). Therefore, Silva et al. (2020) use SDTs as policies which are discretized post-hoc to allow an easy interpretation.

We further included an MLP and SDT as full-complexity models, providing an orientation to state-of-the-art results.

Evaluation procedure. We report the average undiscounted cumulative reward over 5 random trainings with 5 random evaluation episodes each (=25 evaluations for each method). We trained each method for 1mio timesteps. For SYMPOL, SDT and MLP, we optimized the hyperparameters based on the validation reward with optuna (Akiba et al., 2019) for 60 trials using a predefined grid. For D-SDT we discretized the SDT and for SA-DT, we distilled the MLP with the highest performance. More details on the methods and the parameter grids, including the final parameters for each method, are listed in Appendix C.

5.2 RESULTS

SYMPOL learns accurate DT policies. We evaluated our approach against existing methods on control environments in Table 1. SYMPOL is consistently among the best interpretable models and achieves significantly higher rewards compared to alternative methods for learning DT policies on several environments, especially on LL and PD-C. Further, SYMPOL consistently solves CP and AB and is competitive to full-complexity models on most environments.

DT policies offer a good inductive bias for categorical environments. While SYMPOL achieves great results in control benchmarks, it may not be an ideal method for environments modeling physical relationships. As recently also noted by Fuhrer et al. (2024), tree-based models are best suited for categorical environments due to their effective use of axis-aligned splits. In our experiments on MiniGrid (Table 2), SYMPOL achieves comparable or superior results to full-complexity models (e.g. on LG-7). The performance gap between SA-DT and SYMPOL is smaller in certain MiniGrid environments due to less complex environment transition functions and missing randomness, making the distillation easy. Considering more complex environments with randomness or lava like E-R or LG-7, SYMPOL outperforms alternative methods by a substantial margin.

Table 1: **Control Performance.** We report the average undiscounted cumulative test reward over 25 random trials. The best interpretable method, and methods not statistically different, are marked bold.

	CP	AB	LL	MC-C	PD-C
SYMPOL (ours)	500	- 80	- 57	94	- 323
D-SDT	128	-205	-221	-10	-1343
SA-DT (d=5)	446	-97	-197	97	-1251
SA-DT (d=8)	476	- 75	-150	96	- 854
MLP	500	- 72	241	95	- 191
SDT	500	- 77	-124	- 4	- 310

Table 2: **MiniGrid Performance.** We report the average undiscounted cumulative test reward over 25 random trials. The best interpretable method, and methods not statistically different, are marked bold.

	E-R	DK	LG-5	LG-7	DS
SYMPOL (ours)	0.964	0.959	0.951	0.953	0.939
D-SDT	0.662	0.654	0.262	0.381	0.932
SA-DT (d=5)	0.583	0.958	0.951	0.458	0.952
SA-DT (d=8)	0.845	0.961	0.951	0.799	0.954
MLP	0.963	0.963	0.951	0.760	0.951
SDT	0.966	0.959	0.839	0.953	0.954

SYMPOL does not exhibit information loss. Existing methods for learning DT policies usually involve post-processing to obtain the interpretable model. Therefore, they introduce a mismatch between the optimized and interpreted policy, which can result in information loss. An example is given in Figure 1 and more examples are in Figure 12-16. The main advantage of SYMPOL is the direct optimization of a DT policy, which guarantees that there is no information loss between the optimized and interpreted policy. To show this, we calculated Cohens’s D to measure the effect size comparing the validation reward of the trained model with the test reward of the applied, optionally post-processed model (Table 3). We can observe very large effects for SA-DT and D-SDT and only a very small effect for SYMPOL, similar to full-complexity models MLP and SDT.

DT policies learned with SYMPOL are small and interpretable.

While we trained SYMPOL with a depth of 7 and therefore 255 possible nodes, the effective tree size after pruning is significantly smaller with only 50.5 nodes (internal and leaf combined) on average. This can be attributed to a self-pruning mechanism that is inherently applied by SYMPOL in learning redundant paths during the training and therefore only optimizing relevant parts. Furthermore, DTs learned with SYMPOL are smaller than SA-

DTs (d=5) with an average of 60.3 nodes and significantly smaller than SA-DTs (d=8) averaging 291.6 nodes. The pruned D-SDTs are significantly smaller with only 16.5, but also have a very poor performance, as shown in the previous experiment. An exemplary DT learned by SYMPOL, showcasing its interpretability, is visualized in Figure 4. Extended results are in Table 6.

SYMPOL is efficient. In RL, especially for smaller policies, the runtime is mainly determined by the actor-environment interaction. Therefore, recent research put much effort into optimizing this interaction through environment vectorization. The design of SYMPOL, in contrast to existing methods for tree-based RL, allows a flawless integration with these highly efficient training frameworks. As a result, the runtime of SYMPOL is almost identical to using an MLP or SDT as policy, averaging less than 30 seconds for 1mio timesteps. Detailed runtimes are reported in Table 8 and training curves are visualized in Figure 10-11.

Ablation study. In Section 4, we introduced several crucial components to facilitate an efficient and stable training of SYMPOL. To support the intuitive justifications for our modifications, we performed an ablation study (Figure 5) to evaluate the relevance of the individual components. Based on these results, we can confirm that each component substantially contributes to the overall performance.

Table 3: Information Loss. We calculated Cohens’s D to measure effect size between the validation reward of the trained model and the test reward of the applied model. Typically, values > 0.8 are considered as a large effect.

	Cohen’s D \downarrow
SYMPOL (ours)	-0.019
SA-DT (d=5)	3.449
SA-DT (d=8)	2.527
D-SDT	3.126
MLP	0.306
SDT	0.040

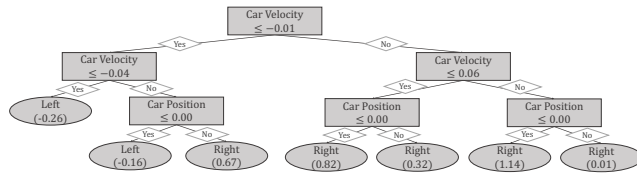


Figure 4: SYMPOL Policy for MountainCar. The main rule encoded by this tree is that the car should accelerate to the left, if its velocity is negative and to the right if it is positive, which essentially increases the speed of the car over time, making it possible to reach the goal at the top of the hill. The magnitude of the acceleration is mainly determined by the current position, reducing the cost of the actions.

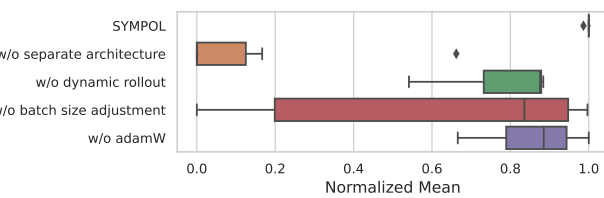


Figure 5: Ablation Study. We report the mean normalized performance over all control environments. Detailed results are reported in Table 7

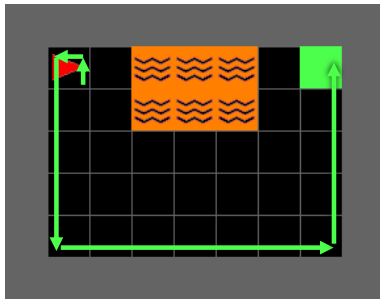


Figure 6: **DistShift**. We show the training environment for the agent along with the starting position and goal. The path taken by SYMPOL (visualized in Figure 7) is marked by green arrows and solves the environment.

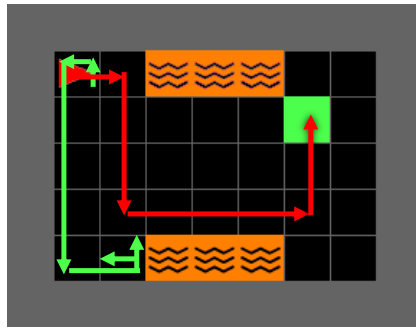


Figure 8: **DistShift with Domain Randomization.** This is a modified version of the DistShift, with the goal and lava at random positions. SYMPOL (Figure 7), visualized as the green line, is not able to solve the randomized environment. Training SYMPOL with domain randomization (Figure 9), visualized as the red line, is able to solve the environment.

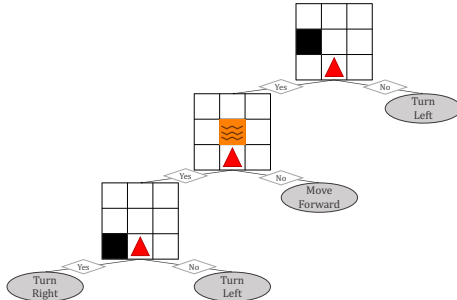


Figure 7: **SYMPOL Policy.** This image shows the DT policy of SYMPOL. The split nodes are visualized as the 3x3 view grid of the agent with one square marking the considered object and position. If the visualized object is present at this position, the true path (left) is taken.

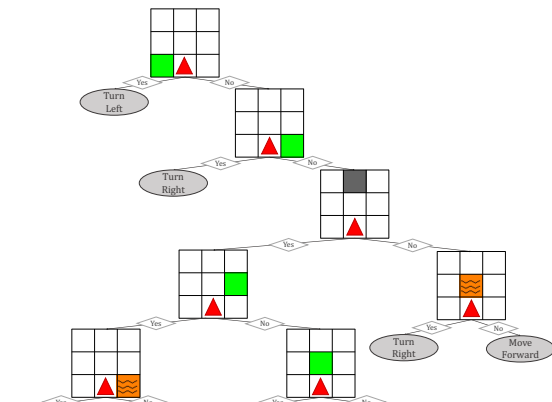


Figure 9: **SYMPOL Policy with Domain Randomization.** The SYMPOL policy (Figure 9) retrained with domain randomization. The agent now has learned to avoid lava and walls, as well as identifying and walk into the goal.

6 CASE STUDY: GOAL MISGENERALIZATION

To demonstrate the benefits of SYMPOLs enhanced transparency, we present a case study on goal misgeneralization (Di Langosco et al., 2022). Good policy generalization is vital in RL, yet agents often exhibit poor out-of-distribution performance, even with minor environmental changes. Goal misgeneralization is a well-researched out-of-distribution robustness failure that occurs when an agent learns robust skills during training but follows unintended goals. This happens when the agent’s behavioral objective diverges from the intended objective, leading to high rewards during training but poor generalization during testing.

To demonstrate that SYMPOL can help in detecting misaligned behavior, let us consider the Dist-Shift environment from MiniGrid, shown in Figure 6. The environment is designed to test for misgeneralization (Chevalier-Boisvert et al., 2023), as the goal is repeatedly placed in the top right corner and the lava remains at the same position. We can formulate the intended behavior according to the task description as avoiding the lava and reaching a specific goal location. SYMPOL, similar to other methods, solved the task consistently. The advantage of SYMPOL is the tree-based structure, which is easily interpretable. When inspecting the SYMPOL policy (Figure 7), we can immediately observe that the agent has not captured the actual task correctly. Essentially, it has only

learned to keep an empty space on the left of the agent (which translates into following the wall) and not to step into lava (but not to get around it). While this is sufficient to solve this exact environment, it is evident, that the agent has not generalized to the overall goal.

In order to test for misgeneralization, we created test environments in which the agent has to reach a random goal placed with lava placed at a varying locations. As already identified based on the interpretable policy, we can observe in Figure 8 that the agent gets stuck when the goal or lava positions change. Alternative non-interpretable policies exhibit the same behavior, which might remain unnoticed due to the black-box nature. Instead of simply looking at the learned policy with SYMPOL, alternative methods would require using external methods or designing complex test cases to detect such misbehavior. Alternative methods to generate DT policies like SA-DT also provide an interpretable policy, but as already shown during our experiments, frequently come with severe information loss. Due to this information loss, we cannot ensure that we are actually interpreting the policy, which is guaranteed using SYMPOL.

Based on these insights, we retrained SYMPOL with domain randomization. The resulting policy (see Figure 9) now solves the randomized environments (see Figure 8), still maintaining interpretability.

7 CONCLUSION AND FUTURE WORK

In this paper, we introduced SYMPOL, a novel method for tree-based RL. SYMPOL can be seamlessly integrated into existing actor-critic RL frameworks, where the DT policy is directly optimized using policy gradients while maintaining interpretability. This direct optimization guarantees that the explanation exactly matches the policy learned during training, avoiding the information loss often encountered with existing methods that rely on post-processing to obtain an interpretable policy. Furthermore, the performance of interpretable DT policies learned by SYMPOL is significantly higher compared to existing methods, particularly in environments involving more complex environment transition functions or randomness. We believe that SYMPOL represents a significant step towards bridging the gap between the performance of actor-critic RL and the interpretability and transparency of symbolic approaches, paving the way for the widespread adoption of trustworthy and explainable AI systems in safety-critical and high-stakes domains.

While we focused on PPO as the state-of-the-art actor-critic RL method, the flexibility of SYMPOL allows an integration into arbitrary RL frameworks, which can be explored in future work. Also, it would be interesting to evaluate a more complex, forest-like tree structure as a performance-interpretability trade-off, similar to Marton et al. (2024b), especially based on the promising results of Fuhrer et al. (2024) for tree-based RL.

REFERENCES

Takuya Akiba, Shotaro Sano, Toshihiko Yanase, Takeru Ohta, and Masanori Koyama. Optuna: A next-generation hyperparameter optimization framework. In *Proceedings of the 25th ACM SIGKDD international conference on knowledge discovery & data mining*, pp. 2623–2631, 2019.

Osbert Bastani, Yewen Pu, and Armando Solar-Lezama. Verifiable reinforcement learning via policy extraction. *Advances in Neural Information Processing Systems*, 31, 2018.

Yoshua Bengio, Nicholas Léonard, and Aaron Courville. Estimating or propagating gradients through stochastic neurons for conditional computation. *arXiv preprint arXiv:1308.3432*, 2013.

Clément Bonnet, Daniel Luo, Donal Byrne, Shikha Surana, Sasha Abramowitz, Paul Duckworth, Vincent Coyette, Laurence I. Midgley, Elshadai Tegegn, Tristan Kalloniatis, Omayma Mahjoub, Matthew Macfarlane, Andries P. Smit, Nathan Grinsztajn, Raphael Boige, Cemlyn N. Waters, Mohamed A. Mimouni, Ulrich A. Mbou Sob, Ruan de Kock, Siddarth Singh, Daniel Furelos-Blanco, Victor Le, Arnu Pretorius, and Alexandre Laterre. Jumanji: a diverse suite of scalable reinforcement learning environments in jax, 2024. URL <https://arxiv.org/abs/2306.09884>.

Chun-Hao Chang, Rich Caruana, and Anna Goldenberg. Node-gam: Neural generalized additive model for interpretable deep learning. *arXiv preprint arXiv:2106.01613*, 2021.

Maxime Chevalier-Boisvert, Bolun Dai, Mark Towers, Rodrigo de Lazcano, Lucas Willems, Salem Lahlou, Suman Pal, Pablo Samuel Castro, and Jordan Terry. Minigrid & miniworld: Modular & customizable reinforcement learning environments for goal-oriented tasks. *CoRR*, abs/2306.13831, 2023.

Youri Coppens, Kyriakos Efthymiadis, Tom Lenaerts, Ann Nowé, Tim Miller, Rosina Weber, and Daniele Magazzeni. Distilling deep reinforcement learning policies in soft decision trees. In *Proceedings of the IJCAI 2019 workshop on explainable artificial intelligence*, pp. 1–6, 2019.

Vinícius G Costa, Jorge Pérez-Aracil, Sancho Salcedo-Sanz, and Carlos E Pedreira. Evolving interpretable decision trees for reinforcement learning. *Artificial Intelligence*, 327:104057, 2024.

Leonardo L Custode and Giovanni Iacca. Evolutionary learning of interpretable decision trees. *IEEE Access*, 11:6169–6184, 2023.

Quentin Delfosse, Hikaru Shindo, Devendra Dhami, and Kristian Kersting. Interpretable and explainable logical policies via neurally guided symbolic abstraction. *Advances in Neural Information Processing Systems*, 36, 2024.

Lauro Langosco Di Langosco, Jack Koch, Lee D Sharkey, Jacob Pfau, and David Krueger. Goal mis-generalization in deep reinforcement learning. In *International Conference on Machine Learning*, pp. 12004–12019. PMLR, 2022.

Damien Ernst, Pierre Geurts, and Louis Wehenkel. Tree-based batch mode reinforcement learning. *Journal of Machine Learning Research*, 6:503–556, 2005.

Benjamin Fuhrer, Chen Tessler, and Gal Dalal. Gradient boosting reinforcement learning. *arXiv preprint arXiv:2407.08250*, 2024.

Jiaming Guo, Rui Zhang, Shaohui Peng, Qi Yi, Xing Hu, Ruizhi Chen, Zidong Du, Ling Li, Qi Guo, Yunji Chen, et al. Efficient symbolic policy learning with differentiable symbolic expression. *Advances in Neural Information Processing Systems*, 36, 2024.

Jiaming Guo et al. Efficient symbolic policy learning with differentiable symbolic expression. *arXiv preprint arXiv:2311.02104*, 2023.

Ujjwal Das Gupta, Erik Talvitie, and Michael Bowling. Policy tree: Adaptive representation for policy gradient. In *Proceedings of the AAAI Conference on Artificial Intelligence*, volume 29, 2015.

Pavel Izmailov, Dmitrii Podoprikin, Timur Garipov, Dmitry Vetrov, and Andrew Gordon Wilson. Averaging weights leads to wider optima and better generalization. *arXiv preprint arXiv:1803.05407*, 2018.

Aman Jhunjhunwala, Jaeyoung Lee, Sean Sedwards, Vahdat Abdelzad, and Krzysztof Czarnecki. Improved policy extraction via online q-value distillation. In *2020 International Joint Conference on Neural Networks (IJCNN)*, pp. 1–8. IEEE, 2020.

Akansha Kalra and Daniel S Brown. Interpretable reward learning via differentiable decision trees. In *NeurIPS ML Safety Workshop*, 2022.

Akansha Kalra and Daniel S Brown. Can differentiable decision trees learn interpretable reward functions? *arXiv preprint arXiv:2306.13004*, 2023.

Kentaro Kanamori, Takuya Takagi, Ken Kobayashi, and Yuichi Ike. Counterfactual explanation trees: Transparent and consistent actionable recourse with decision trees. In *International Conference on Artificial Intelligence and Statistics*, pp. 1846–1870. PMLR, 2022.

Diederik P Kingma and Jimmy Ba. Adam: A method for stochastic optimization. *arXiv preprint arXiv:1412.6980*, 2014.

Mikel Landajuela, Brenden K Petersen, Sookyung Kim, Claudio P Santiago, Ruben Glatt, T Nathan Mundhenk, Jacob F Pettit, and Daniel M Faißol. Discovering symbolic policies with deep reinforcement learning. In *Proceedings of the 38th International Conference on Machine Learning*, pp. 5979–5989. PMLR, 2021.

Robert Tjarko Lange. gymnas: A JAX-based reinforcement learning environment library, 2022.
URL <http://github.com/RobertTLange/gymnas>.

Zhao-Hua Li, Yang Yu, Yingfeng Chen, Ke Chen, Zhipeng Hu, and Changjie Fan. Neural-to-tree policy distillation with policy improvement criterion. *arXiv preprint arXiv:2108.06898*, 2021.

Guiliang Liu, Oliver Schulte, Wang Zhu, and Qingcan Li. Toward interpretable deep reinforcement learning with linear model u-trees. In *Machine Learning and Knowledge Discovery in Databases: European Conference, ECML PKDD 2018, Dublin, Ireland, September 10–14, 2018, Proceedings, Part II* 18, pp. 414–429. Springer, 2019.

Xiao Liu, Shuyang Liu, Bo An, Yang Gao, Shangdong Yang, and Wenbin Li. Effective interpretable policy distillation via critical experience point identification. *IEEE Intelligent Systems*, 38(5): 28–36, 2023.

Ilya Loshchilov and Frank Hutter. Decoupled weight decay regularization. *arXiv preprint arXiv:1711.05101*, 2017.

Lirui Luo et al. End-to-end neuro-symbolic reinforcement learning with textual explanations. *arXiv preprint arXiv:2403.12451*, 2024.

Sascha Marton, Stefan Lüdtke, Christian Bartelt, and Heiner Stuckenschmidt. Gradtree: Learning axis-aligned decision trees with gradient descent. In *Proceedings of the AAAI Conference on Artificial Intelligence*, volume 38, pp. 14323–14331, 2024a.

Sascha Marton, Stefan Lüdtke, Christian Bartelt, and Heiner Stuckenschmidt. Grande: Gradient-based decision tree ensembles for tabular data. In *The Twelfth International Conference on Learning Representations*, 2024b.

Stephanie Milani, Zhicheng Zhang, Nicholay Topin, Zheyuan Ryan Shi, Charles Kamhoua, Evangelos E Papalexakis, and Fei Fang. Maviper: Learning decision tree policies for interpretable multi-agent reinforcement learning. In *Joint European Conference on Machine Learning and Knowledge Discovery in Databases*, pp. 251–266. Springer, 2022.

Joosung Min and Lloyd T Elliott. Q-learning with online random forests. *arXiv preprint arXiv:2204.03771*, 2022.

Svetlin Penkov and Subramanian Ramamoorthy. Learning programmatically structured representations with perceptor gradients. *arXiv preprint arXiv:1905.00956*, 2019.

Ben Peters, Vlad Niculae, and André FT Martins. Sparse sequence-to-sequence models. *arXiv preprint arXiv:1905.05702*, 2019.

Sergei Popov, Stanislav Morozov, and Artem Babenko. Neural oblivious decision ensembles for deep learning on tabular data. *arXiv preprint arXiv:1909.06312*, 2019.

Aaron M Roth, Nicholay Topin, Pooyan Jamshidi, and Manuela Veloso. Conservative q-improvement: Reinforcement learning for an interpretable decision-tree policy. *arXiv preprint arXiv:1907.01180*, 2019.

John Schulman, Filip Wolski, Prafulla Dhariwal, Alec Radford, and Oleg Klimov. Proximal policy optimization algorithms. *arXiv preprint arXiv:1707.06347*, 2017.

Andrew Silva and Matthew Gombolay. Encoding human domain knowledge to warm start reinforcement learning. In *Proceedings of the AAAI conference on artificial intelligence*, volume 35, pp. 5042–5050, 2021.

Andrew Silva, Matthew Gombolay, Taylor Killian, Ivan Jimenez, and Sung-Hyun Son. Optimization methods for interpretable differentiable decision trees applied to reinforcement learning. In *International conference on artificial intelligence and statistics*, pp. 1855–1865. PMLR, 2020.

Pradyumna Tambwekar, Andrew Silva, Nakul Gopalan, and Matthew Gombolay. Natural language specification of reinforcement learning policies through differentiable decision trees. *IEEE Robotics and Automation Letters*, 8(6):3621–3628, 2023.

Mark Towers, Ariel Kwiatkowski, Jordan Terry, John U Balis, Gianluca De Cola, Tristan Deleu, Manuel Goulão, Andreas Kallinteris, Markus Krimmel, Arjun KG, et al. Gymnasium: A standard interface for reinforcement learning environments. *arXiv preprint arXiv:2407.17032*, 2024.

Dweep Trivedi, Jesse Zhang, Shao-Hua Sun, and Joseph J Lim. Learning to synthesize programs as interpretable and generalizable policies. *Advances in neural information processing systems*, 34: 25146–25163, 2021.

Abhinav Verma, Vijayaraghavan Murali, Rishabh Singh, Pushmeet Kohli, and Swarat Chaudhuri. Programmatically interpretable reinforcement learning. In *International Conference on Machine Learning*, pp. 5045–5054. PMLR, 2018.

Daniël Vos and Sicco Verwer. Optimal decision tree policies for markov decision processes. *arXiv preprint arXiv:2301.13185*, 2023.

Maxime Waburtha and Joelle Pineau. Piecewise linear parametrization of policies: Towards interpretable deep reinforcement learning. In *The Twelfth International Conference on Learning Representations*, 2024. URL <https://openreview.net/forum?id=hOMVq57Ce0>.

Jiayi Weng, Min Lin, Shengyi Huang, Bo Liu, Denys Makoviichuk, Viktor Makoviychuk, Zichen Liu, Yufan Song, Ting Luo, Yukun Jiang, Zhongwen Xu, and Shuicheng Yan. EnvPool: A highly parallel reinforcement learning environment execution engine. In S. Koyejo, S. Mohamed, A. Agarwal, D. Belgrave, K. Cho, and A. Oh (eds.), *Advances in Neural Information Processing Systems*, volume 35, pp. 22409–22421. Curran Associates, Inc., 2022. URL https://proceedings.neurips.cc/paper_files/paper/2022/file/8caaf08e49ddbad6694fae067442ee21-Paper-Datasets_and_Benchmarks.pdf.

Kai Xu et al. Symbolic-model-based reinforcement learning. *arXiv preprint arXiv:2203.12346*, 2022.

Zhuorui Ye, Stephanie Milani, Fei Fang, and Geoff Gordon. Concept-based interpretable reinforcement learning with limited to no human labels. In *Workshop on Interpretable Policies in Reinforcement Learning@ RLC-2024*, 2024.

A ADDITIONAL RESULTS

In this section, we present additional results to support the claims made in the main paper, along with extended results for the summarizing tables. We focus on the control environments because they offer a diverse suite of benchmarks that cover different tasks and include both continuous and discrete action spaces. We chose not to include the MiniGrid environments here because their inclusion could distort the results, particularly the averages calculated in the main paper, as all MiniGrid environments involve similar tasks and feature a discrete action and observation space. The primary reason for including MiniGrid in the main paper is to provide additional experimental results that confirm the robustness and applicability of our method across different domains, as well as to highlight that tree-based methods offer a beneficial inductive bias for these categorical environments.

A.1 INFORMATION LOSS

We provide detailed results on the information loss which can result as a consequence of discretization (for D-SDT) or distillation (for SA-DT). In Table 4, we report the validation reward of the trained model along with the test reward of the discretized model. We can clearly observe that there are major differences for SA-DT and D-SDT on several datasets, indicating information loss. In Table 5, we report Cohen’s D to measure the effect size comparing the validation reward of the trained model with the test reward of the applied, optionally post-processed model. Again, we can clearly see large effects for SA-DT and D-SDT on several datasets, especially for Pendulum (PD-C) and LunarLander (LL), but also CartPole (CP). Furthermore, the training curves in Figure 11 visually show the information loss during the training.

Table 4: **Information Loss (Comparison)**. We report the validation reward of the trained model and the test reward of the applied model.

	MLP		SDT		SYMPOL (ours)		SA-DT (d=5)		SA-DT (d=8)		D-SDT	
	valid	test	valid	test	valid	test	valid	test	valid	test	valid	test
CP	500	500	500	500	500	500	500	446	500	476	500	128
AB	-71	-72	-89	-77	-79	-80	-71	-97	-71	-75	-89	-205
LL	256	241	-91	-124	-9	-57	256	-197	256	-150	-91	-221
MC-C	95	95	-4	-4	87	94	95	97	95	96	-4	-10
PD-C	-169	-191	-295	-310	-305	-323	-169	-1251	-169	-854	-295	-1343

Table 5: **Information Loss (Cohen’s D)**. We calculated Cohens’s D to measure effect size between the validation reward of the trained model and the test reward of the applied model. Typically, values > 0.5 are considered a medium and values > 0.8 a large effect. positive effects that are at least medium are marked as bold.

	MLP	SDT	SYMPOL (ours)	SA-DT (d=5)	SA-DT (d=8)	D-SDT
CP	0.000	0.000	0.000	0.632	1.214	4.075
AB	0.035	-0.630	0.104	0.728	0.338	0.982
LL	0.341	0.750	0.370	4.776	8.155	2.254
MC-C	-0.042	-0.002	-1.035	-2.011	-1.172	0.745
PD-C	1.195	0.081	0.468	13.120	4.101	7.573
Mean \downarrow	0.306	0.040	-0.019	3.449	2.527	3.126

A.2 TREE SIZE

We report the average tree sizes over 25 trials for each environment. The DTs for SYMPOL and D-SDT are automatically pruned by removing redundant paths. There are mainly two identifiers, making a path redundant:

- The split threshold of a split is outside the range specified by the environment. For instance, if $x_1 \in [0.0, 1.0]$ the decision $x_1 \leq -0.1$ will always be false as $-0.1 \leq 0.0$.
- A decision at a higher level of the tree already predefines the current decision. For instance, if the split at the root node is $x_1 \leq 0.5$ and the subsequent node following the true path is $x_1 \leq 0.6$ we know that this node will always be evaluated to true as $0.5 \leq 0.6$.

We excluded the MiniGrid environments here, as they require a more sophisticated, automated pruning as there exist more requirements making a path redundant. For instance, if for the decision whether there is a wall in front of the agent is true, the decision for all other objects at the same position has to be always false.

Table 6: **Tree Size**. We report the average size of the learned DT for each environment.

	SYMPOL (ours)	D-SDT	SA-DT (d=5)	SA-DT (d=8)
CP	39.4	14.2	61.8	315.0
AB	78.6	17.0	56.5	173.0
LL	55.0	19.8	59.8	270.2
MC-C	23.4	3.0	61.0	311.8
PD-C	56.2	28.6	62.2	388.2
Mean \downarrow	50.5	16.5	60.3	291.6

A.3 ABLATION STUDY

Our ablation study was designed to support our intuitive justifications for the modifications made to the RL framework and our method. Therefore, we disabled individual component of our method

and evaluated the performance without the specific component. This includes the following modifications introduced in Section 4:

1. **w/o separate architecture:** Instead of using separate architectures for actor and critic, we use the same architecture and hyperparameters for the actor and critic.
2. **w/o dynamic rollout:** We proposed a dynamic rollout buffer that increases with a stepwise exponential rate during training to increase stability while maintaining exploration early on. Here we used a standard, static rollout buffer.
3. **w/o batch size adjustment:** Similar to the dynamic rollout buffer, we proposed using a dynamic batch size to increase gradient stability in later stages of the training. Here, we used standard, static batch size.
4. **w/o adamW:** We introduced an Adam optimizer with weight decay to SYMPOL to support the adjustment of the features to split on and the class predicted. Here, we use a standard Adam optimizer without weight decay.

Detailed results for each of the control datasets are reported in Table 7. The results clearly confirm our intuitive justifications, as each adjustment has a crucial impact on the performance of SYMPOL.

Table 7: **Ablation Study.** We report the average test performance over a total of 25 random trials. This normalized performance consists in normalizing each reward between 0 and 1 via an affine renormalization between the top- and worse-performing models. Instead of the worse-performing model, we use the 20% test reward quantile to account for outliers.

Agent Type	CP	AB	LL	MC-C	PD-C	Normalized Mean (\uparrow)
SYMPOL	500.0	- 79.9	- 57.4	94.3	- 323.3	0.988
w/o separate architecture	135.6	-196.4	-276.8	-552.4	-1219.4	0.080
w/o dynamic rollout	456.1	- 92.0	-178.2	-144.1	- 434.4	0.598
w/o batch size adjustment	498.8	- 81.7	-320.7	-1818.8	- 434.4	0.372
w/o adamW	416.1	- 78.3	- 97.3	0.0	- 393.5	0.865

A.4 RUNTIME AND TRAINING CURVES

The experiments were conducted on a single NVIDIA RTX A6000. The environments for Cart-Pole (CP), Acrobot (AB), MountainCarContinuous (MC-C) and Pendulum (PD-C) were vectorized (Lange, 2022) and therefore the training is highly efficient, taking only 30 seconds for 1mio timesteps on average (excluding the sequential evaluation which cannot be vectorized). The remaining environments are not vectorized, and we used the standard Gymnasium (Towers et al., 2024) implementation. In Table 8 can clearly see the impact of environment vectorization, as the runtime for LunarLander (LL), which is not vectorized, is more than 10 times higher with over 400 seconds.

Table 8: **Runtime.** We report the average runtime over 25 trials. One trial spans 1mio timesteps for each environment. We excluded LunarLander (LL) from the mean runtime calculation, as this is the only non-vectorized environment. To provide a fair comparison of different methods, we aligned the step and batch size.

	SYMPOL (ours)	SDT	MLP
CP	28.8	23.9	25.2
AB	35.5	37.7	33.8
MC-C	23.4	19.4	18.4
PD-C	28.7	28.2	18.5
Mean \downarrow	29.1	27.3	24.0
LL	402.3	394.0	405.6

In addition to the training times, we report detailed training curves for each method. Figure 10 compares the training reward and the test reward of SYMPOL with the full-complexity models

MLP and SDT. SYMPOL shows a similar convergence compared to full-complexity models on most environments. For Acrobot (AB), SYMPOL converges even faster than an MLP which can be attributed to the dynamic rollout buffer and batch size. For MountainCar (MC-C) we can see that the training of SYMPOL is very unstable at the beginning. We believe that this can be attributed to the sparse reward function of this certain environment and the fact that as a result, minor changes in the policy can result in a severe drop in the reward. Combined with the small rollout buffer and batch size early in the training of SYMPOL, this can result in an unstable training. However, we can see that the training stabilizes later on, which again confirms the design of our dynamic buffer size increasing over time.

Furthermore, we provide a pairwise comparison of SYMPOL with SA-DT and D-SDT in Figure 11. Here, we can again observe the severe information loss for D-SDT and SA-DT by comparing the training curve with the test reward.

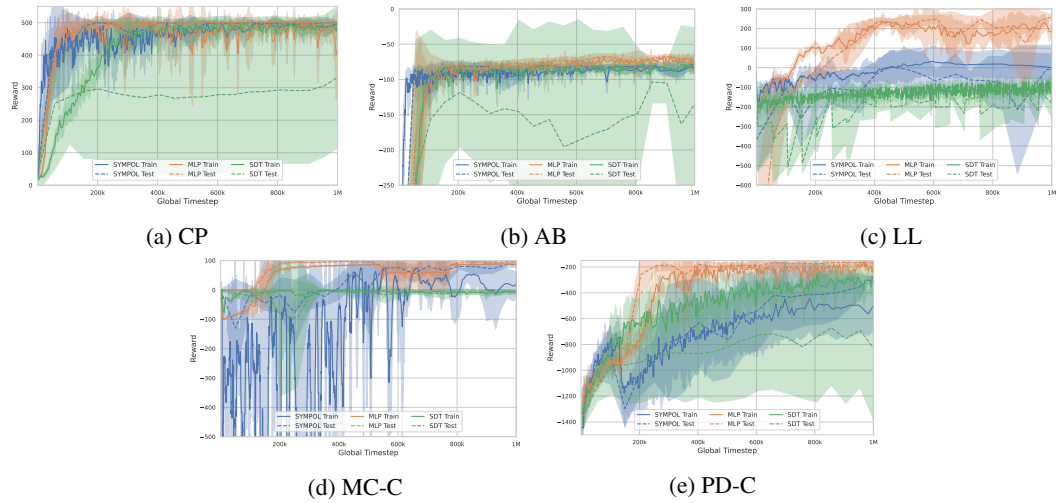


Figure 10: **Training Curves (Full-Complexity).** Shows the training reward as solid line and the test reward as dashed line for SYMPOL (blue), MLP (orange) and SDT (green).

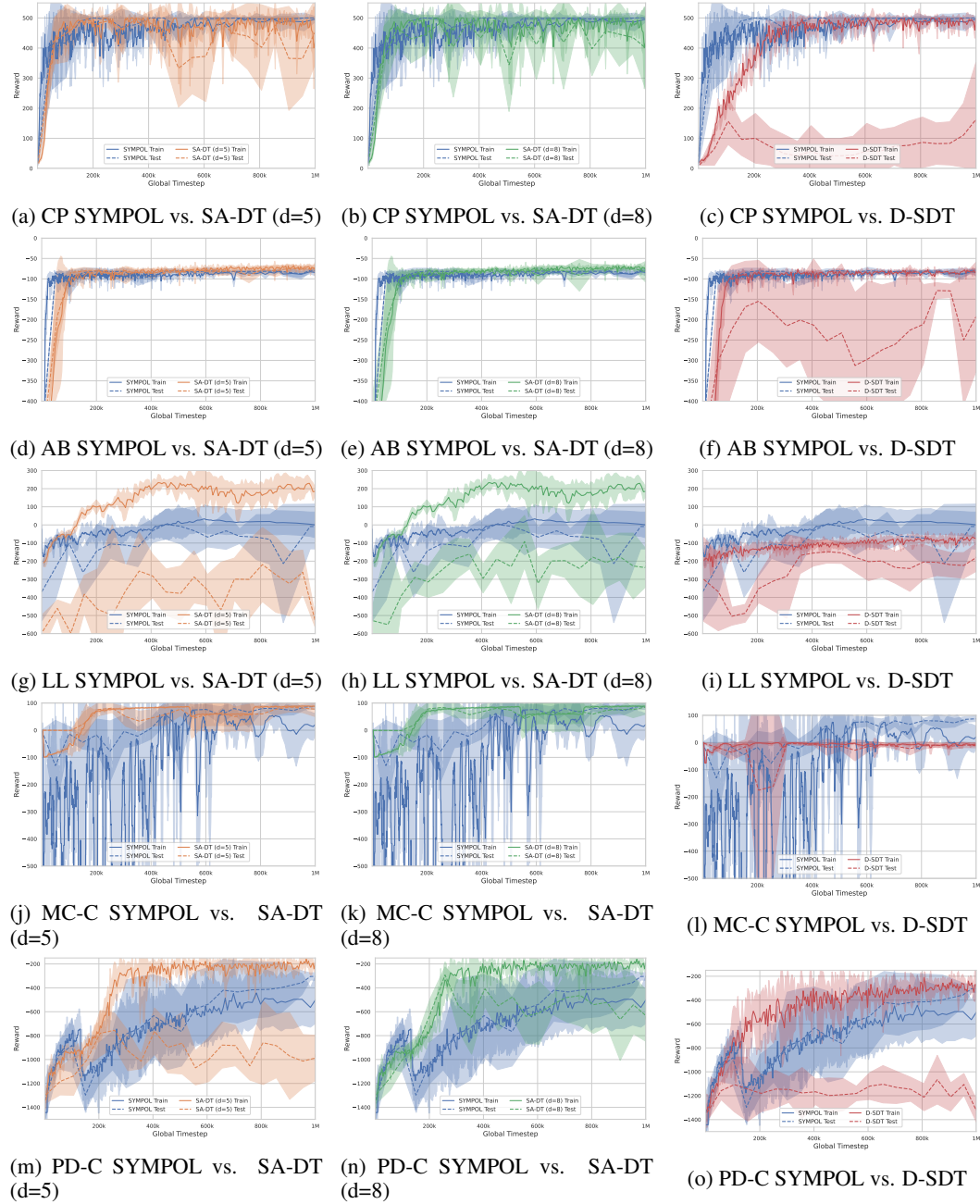


Figure 11: **Training Curves.** Shows the training reward as solid line and the test reward as dashed line for SYMPOL (blue), SA-DT-5 (orange) SA-DT-8 (green) and D-SDT (red). Thereby, the test reward is calculated with the discretized/distilled policy for SA-DT and D-SDT. For several datasets, we can again observe the severe information loss introduced with the post-processing (e.g. for PD-C and LL).

B MINIGRID

We used the MiniGrid implementation from (Chevalier-Boisvert et al., 2023). For each environment, we limited to observations and the actions to the available ones according to the documentation. Furthermore, we decided to use a view size of 3 to allow a good visualization of the results. In the following, we provide more examples for our MiniGrid Use-Case, along with more detailed visual-

izations. In the following, we visualized the SYMPOL agent sequentially acting in the environment as one image for one step from left to right and top to bottom. Figure 12 shows how SYMPOL (see image in the main paper or `tree_function(obs)` defined below) solves the environment. Figure 13 and Figure 15 show the same agent failing on the environment with domain randomization, proving that the agent did not generalize, as we could already observe by inspecting the symbolic, tree-based policy. Retraining the agent with domain randomization (see image in the main paper or `tree_function_retrained(obs)` defined below), SYMPOL is able to solve the environment (see Figure 14 and Figure 16), maintaining interpretability.

B.1 VISUALIZATIONS ENVIRONMENT

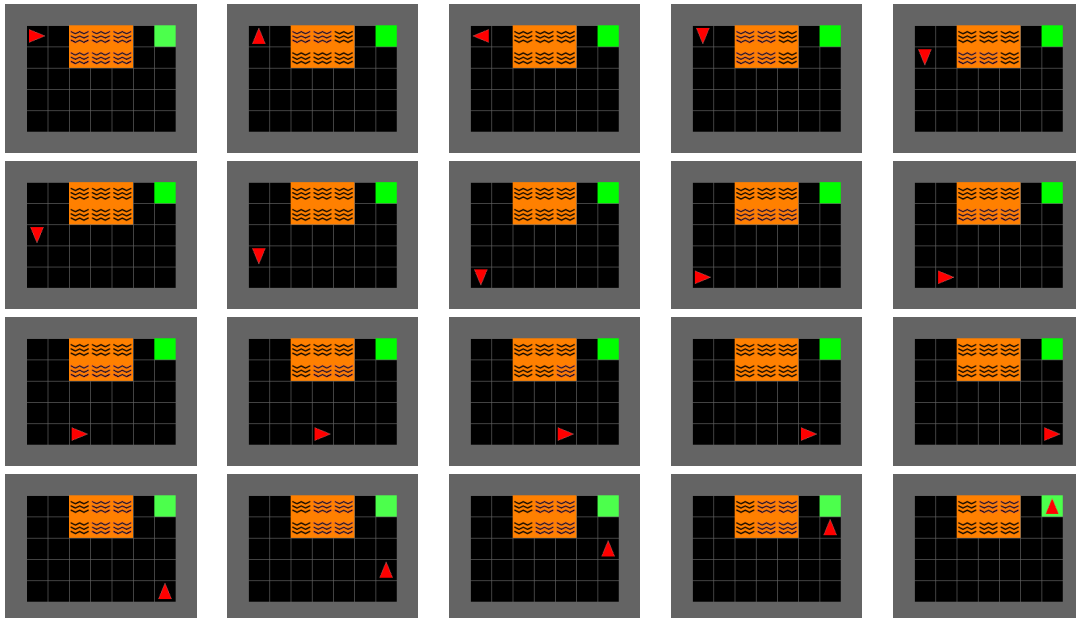


Figure 12: **DistShift SYMPOL.** This figure visualizes the path taken by the SYMPOL agent trained on the basic DistShift environment (see image in the main paper or `tree_function(obs)` defined below) from left to right and top to bottom. The agent follows the wall and reaches the goal at the top right corner.

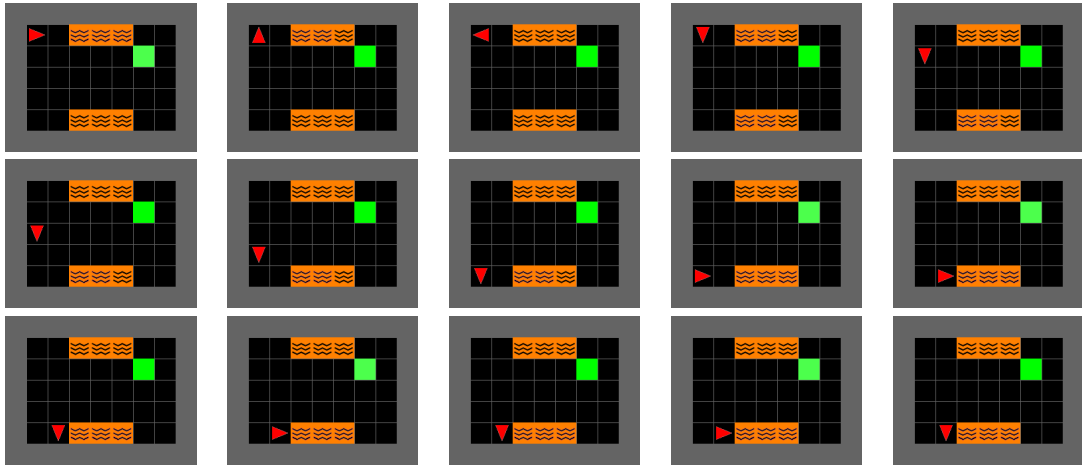


Figure 13: **DistShift (Domain Randomization) SYMPOL Example 1.** This figure visualizes the path taken by the SYMPOL agent trained on the basic DistShift environment (see image in the main paper or `tree_function(obs)` defined below) from left to right and top to bottom. The agent follows the wall gets stuck by the lava.

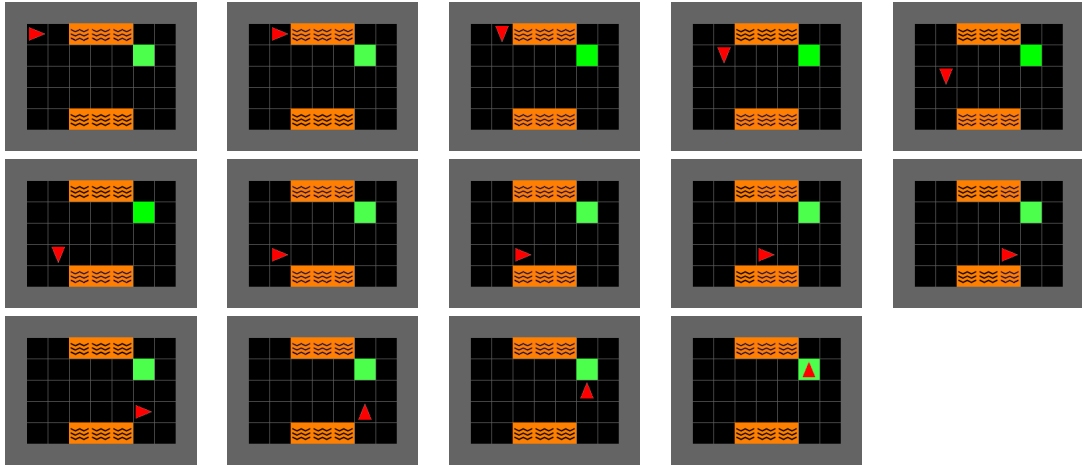


Figure 14: **DistShift (Domain Randomization) SYMPOL (retrained) Example 1.** This figure visualizes the path taken by the SYMPOL agent trained on the randomized DistShift environment (see image in the main paper or `tree_function_retrained(obs)` defined below) from left to right and top to bottom. The agent avoids the lava, identifies the goal and walks into the goal.

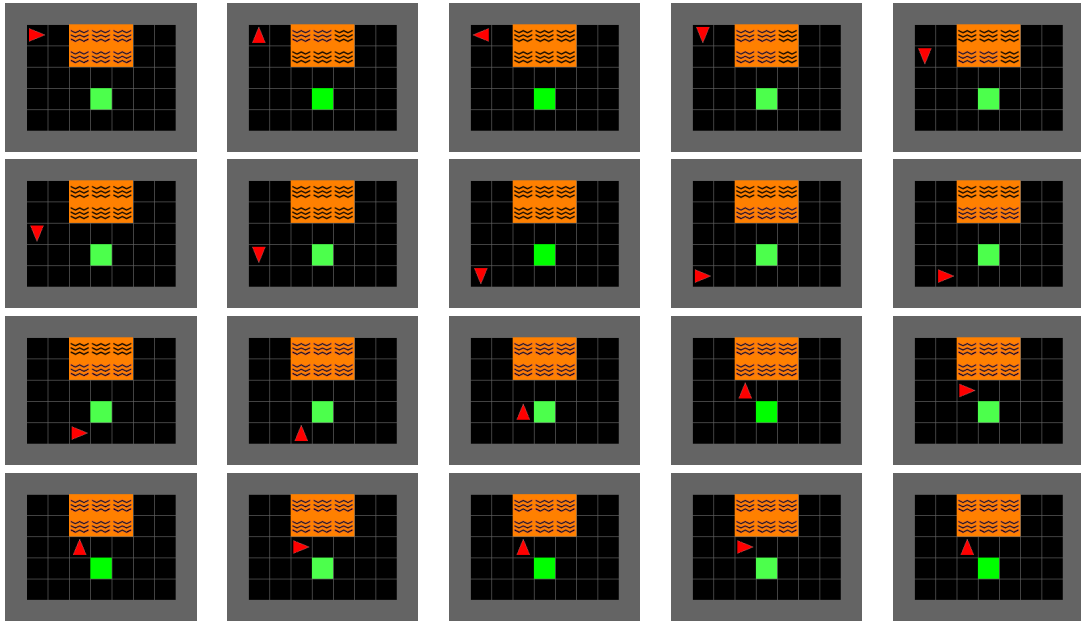


Figure 15: **DistShift (Domain Randomization) SYMPOL Example 2.** This figure visualizes the path taken by the SYMPOL agent trained on the basic DistShift environment (see image in the main paper or `tree_function(obs)` defined below) from left to right and top to bottom. The agent follows the wall until there is no empty space on the left. Instead of an empty space there is the goal, but instead of walking into the goal, the agent surpasses it and again gets stuck at the lava.

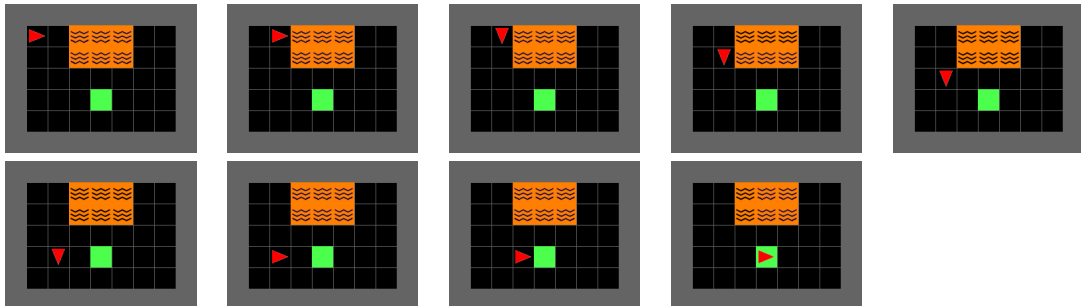


Figure 16: **DistShift (Domain Randomization) SYMPOL (retrained) Example 2.** This figure visualizes the path taken by the SYMPOL agent trained on the randomized DistShift environment (see image in the main paper or `tree_function_retrained(obs)` defined below) from left to right and top to bottom. The agent avoids the lava, identifies the goal, and walks into the goal.

B.2 SYMPOL ALGORITHMIC PRESENTATION

```
1 def tree_function(obs):
2     if obs[field one to front and one to left] is 'empty':
3         if obs[field one to front] is 'lava':
4             if obs[field one to left] is 'empty':
5                 action = 'turn right'
6             else:
7                 action = 'turn left'
8         else:
9             action = 'move forward'
10    else:
11        action = 'turn left'
12    return action
```

```
1 def tree_function_retrained(obs):
2     if obs[field one to left] is 'goal':
3         action = 'turn left'
4     else:
5         if obs[field one to right] is 'goal':
6             action = 'turn right'
7         else:
8             if obs[field two to front] is 'wall':
9                 if obs[field one to front and one to right] is 'goal':
10                     if obs[field one to right] is 'lava':
11                         action = 'turn left'
12                     else:
13                         action = 'move forward'
14                 else:
15                     if obs[field one to front] is 'goal':
16                         action = 'move forward'
17                     else:
18                         action = 'turn left'
19             else:
20                 if obs[field one to front] is 'lava':
21                     action = 'turn right'
22                 else:
23                     action = 'move forward'
24    return action
```

C METHODS AND HYPERPARAMETERS

The main methods we compared SYMPOL against are behavioral cloning state-action DTs (SA-DT) and discretized soft decision trees (D-SDT). In addition to the information given in the paper, we want to provide some more detailed results of the implementation and refer to our source code for the exact definition.

- **State-Action DTs (SA-DT)** Behavioral cloning SA-DTs are the most common method to generate interpretable policies post-hoc. Hereby, we first train an MLP policy, which is then distilled into a DT as a post-processing step after the training. Specifically, we train the DT on a dataset of expert trajectories generated with the MLP policy. The number of expert trajectories was set to 25 which we experienced as a good trade-off between dataset size for the distillation and model complexity during preliminary experiments. The 25 expert trajectories result in a total of approximately 12500 state-action pairs, varying based on the environment specification.
- **Discretized Soft Decision Trees (D-SDT)** SDTs allow gradient computation by assigning probabilities to each node. While SDTs exhibit a hierarchical structure, they are usually considered as less interpretable, since multiple features are considered in a single split and the whole tree is traversed simultaneously (Marton et al., 2024a). Therefore, Silva et al. (2020) use SDTs as policies which are discretized post-hoc to allow an easy interpretation considering only a single feature at each split. Discretization is achieved by employing an argmax to obtain the feature index and normalizing the split threshold based on the feature vector. We improved their method by replacing the scaled sigmoid and softmax, with an entmoid and entmax transformation (Peters et al., 2019), resulting in sparse feature selectors with more responsive gradients, as it is common practice Popov et al. (2019); Chang et al. (2021).

In the following, we list the parameter grids used during the hyperparameter optimization (HPO) as well as the optimal parameters selected for each environment. For SYMPOL, SDT and MLP, we optimized the hyperparameters based on the validation reward with optuna Akiba et al., 2019 for 60 trials. Thereby, we ensured that the environments evaluated during the HPO were distinct to the environments used for reporting the test performance in the rest of the paper.

C.1 HPO GRIDS

Table 9: **HPO Grid MLP**

hyperparameter	values
neurons_per_layer	[16, 256]
num_layers	[1, 3]
learning_rate_actor	[0.0001, 0.01]
learning_rate_critic	[0.0001, 0.01]
minibatch_size	{64, 128, 256, 512}
n_update_epochs	[1, 10]
n_steps	{128, 512}
n_envs	[4, 16]
norm_adv	{True, False}
ent_coef	{0.0, 0.1, 0.2, 0.5}
gae_lambda	{0.8, 0.9, 0.95, 0.99}
gamma	{0.9, 0.95, 0.99, 0.999}
vf_coef	{0.25, 0.50, 0.75}
max_grad_norm	{0.1, 0.5, 1.0, None}

Table 10: **HPO Grid SYMPOL**

hyperparameter	values
learning_rate_actor_weights	[0.0001, 0.1]
learning_rate_actor_split_values	[0.0001, 0.05]
learning_rate_actor_split_idx_array	[0.0001, 0.1]
learning_rate_actor_leaf_array	[0.0001, 0.05]
learning_rate_actor_log_std	[0.0001, 0.1]
learning_rate_critic	[0.0001, 0.01]
n_update_epochs	[0, 10]
reduce_lr	{True, False}
n_steps	{128, 512}
n_envs	[4, 16]
norm_adv	{True, False}
ent_coef	{0.0, 0.1, 0.2, 0.5}
gae_lambda	{0.8, 0.9, 0.95, 0.99}
gamma	{0.9, 0.95, 0.99, 0.999}
vf_coef	{0.25, 0.50, 0.75}
max_grad_norm	[None]
SWA	{True}
adamW	{True}
depth	{7}
minibatch_size	{64}

Table 11: **HPO Grid SDT**

hyperparameter	values
critic	{'MLP', 'SDT'}
depth	[4, 8]
temperature	{0.01, 0.05, 0.1, 0.5, 1.0}
learning_rate_actor	[0.0001, 0.01]
learning_rate_critic	[0.0001, 0.01]
minibatch_size	{64, 128, 256, 512}
n_update_epochs	[1, 10]
n_steps	{128, 512}
n_envs	[4, 16]
norm_adv	{True, False}
ent_coef	{0.0, 0.1, 0.2, 0.5}
gae_lambda	{0.8, 0.9, 0.95, 0.99}
gamma	{0.9, 0.95, 0.99, 0.999}
vf_coef	{0.25, 0.50, 0.75}
max_grad_norm	{0.1, 0.5, 1.0, None}

C.2 BEST HYPERPARAMETERS

Table 12: **Best Hyperparameters MLP (Control)**

	CP	AB	LL	MC-C	PD-C
adamW	False	False	False	False	False
ent_coef	0.200	0.000	0.100	0.100	0.100
gae_lambda	0.900	0.900	0.900	0.950	0.950
gamma	0.999	0.990	0.999	0.999	0.990
learning_rate_actor	0.001	0.000	0.001	0.005	0.000
learning_rate_critic	0.003	0.005	0.003	0.001	0.002
max_grad_norm	1.000	1.000	0.500	0.100	None
minibatch_size	256	256	128	512	128
n_envs	13	12	13	15	8
n_steps	128	512	512	512	512
n_update_epochs	7	9	8	2	2
neurons_per_layer	139	185	46	240	75
norm_adv	False	True	False	True	True
num_layers	2	2	3	2	2
reduce_lr	False	False	False	False	False
vf_coef	0.250	0.500	0.500	0.250	0.250

Table 13: **Best Hyperparameters MLP (MiniGrid)**

	E-R	DK	LG-5	LG-7	DS
adamW	False	False	False	False	False
ent_coef	0.100	0.100	0.100	0.100	0.100
gae_lambda	0.950	0.900	0.950	0.950	0.990
gamma	0.990	0.900	0.990	0.900	0.990
learning_rate_actor	0.000	0.000	0.002	0.000	0.000
learning_rate_critic	0.001	0.000	0.003	0.001	0.001
max_grad_norm	0.100	0.100	1	0.500	0.100
minibatch_size	64	256	128	512	256
n_envs	13	8	8	12	10
n_steps	512	256	512	128	128
n_update_epochs	5	7	9	8	7
neurons_per_layer	112	169	76	28	158
norm_adv	False	True	False	True	True
num_layers	3	1	1	1	2
reduce_lr	False	False	False	False	False
vf_coef	0.500	0.500	0.250	0.750	0.500

Table 14: **Best Hyperparameters SYMPOL (Control)**

	CP	AB	LL	MC-C	PD-C
ent_coef	0.200	0.000	0.000	0.500	0.100
gae_lambda	0.950	0.950	0.900	0.990	0.800
gamma	0.990	0.990	0.999	0.999	0.999
learning_rate_actor_weights	0.048	0.003	0.072	0.000	0.022
learning_rate_actor_split_values	0.000	0.000	0.001	0.000	0.000
learning_rate_actor_split_idx_array	0.026	0.052	0.010	0.000	0.010
learning_rate_actor_leaf_array	0.020	0.005	0.009	0.028	0.006
learning_rate_actor_log_std	0.001	0.002	0.021	0.094	0.000
learning_rate_critic	0.001	0.000	0.002	0.002	0.000
max_grad_norm	None	None	None	None	None
n_envs	7	8	6	5	15
n_steps	512	128	512	128	128
n_update_epochs	7	7	7	2	7
norm_adv	False	False	True	False	True
reduce_lr	True	True	True	True	False
vf_coef	0.500	0.250	0.500	0.500	0.750
SWA	True	True	True	True	True
adamW	True	True	True	True	True
dropout	0.000	0.000	0.000	0.000	0.000
depth	7	7	7	7	7
minibatch_size	64	64	64	64	64
n_estimators	1	1	1	1	1

Table 15: **Best Hyperparameters SYMPOL (MiniGrid)**

	E-R	DK	LG-5	LG-7	DS
ent_coef	0.100	0.200	0.100	0.100	0.500
gae_lambda	0.990	0.950	0.900	0.900	0.950
gamma	0.900	0.990	0.950	0.990	0.999
learning_rate_actor_weights	0.063	0.042	0.055	0.001	0.036
learning_rate_actor_split_values	0.001	0.001	0.006	0.001	0.000
learning_rate_actor_split_idx_array	0.001	0.001	0.012	0.001	0.009
learning_rate_actor_leaf_array	0.003	0.004	0.009	0.008	0.001
learning_rate_actor_log_std	0.043	0.021	0.005	0.002	0.038
learning_rate_critic	0.001	0.001	0.001	0.001	0.001
max_grad_norm	None	None	None	None	None
n_envs	14	14	16	7	10
n_steps	128	512	512	128	512
n_update_epochs	8	9	5	4	5
norm_adv	True	True	True	True	False
reduce_lr	False	True	True	True	True
vf_coef	0.500	0.500	0.250	0.500	0.250
SWA	True	True	True	True	True
adamW	True	True	True	True	True
dropout	0.000	0.000	0.000	0.000	0.000
depth	7	7	7	7	7
minibatch_size	64	64	64	64	64
n_estimators	1	1	1	1	1

Table 16: **Best Hyperparameters SDT (Control)**

	CP	AB	LL	MC-C	PD-C
adamW	False	False	False	False	False
critic	mlp	mlp	mlp	mlp	mlp
depth	7	6	8	7	7
ent_coef	0.000	0.100	0.200	0.000	0.200
gae_lambda	0.950	0.950	0.990	0.900	0.900
gamma	0.990	0.990	0.999	0.990	0.900
learning_rate_actor	0.001	0.002	0.001	0.001	0.000
learning_rate_critic	0.000	0.000	0.001	0.007	0.000
max_grad_norm	0.100	0.100	1.000	0.500	0.100
minibatch_size	128	128	128	64	128
n_envs	15	6	7	14	7
n_steps	512	128	512	512	256
n_update_epochs	4	10	2	1	7
norm_adv	True	False	True	False	False
reduce_lr	False	False	False	False	False
temperature	1	0.500	1	1	0.100
vf_coef	0.500	0.500	0.750	0.250	0.500

Table 17: **Best Hyperparameters SDT (MiniGrid)**

	E-R	DK	LG-5	LG-7	DS
adamW	False	False	False	False	False
critic	sdt	mlp	sdt	sdt	sdt
depth	7	6	7	8	7
ent_coef	0.100	0.100	0.200	0.100	0.100
gae_lambda	0.900	0.950	0.990	0.950	0.900
gamma	0.990	0.900	0.999	0.950	0.950
learning_rate_actor	0.004	0.001	0.000	0.002	0.001
learning_rate_critic	0.000	0.002	0.000	0.005	0.002
max_grad_norm	0.100	0.100	0.500	0.100	None
minibatch_size	512	256	512	256	512
n_envs	10	10	10	13	5
n_steps	512	256	256	128	512
n_update_epochs	5	10	8	4	7
norm_adv	True	True	True	True	True
reduce_lr	False	False	False	False	False
temperature	1	1	1	1	1
vf_coef	0.750	0.750	0.750	0.250	0.750